Depolarization-Induced Slowing of Ca^{2+} Channel Deactivation in Squid Neurons

Matthew B. McFarlane
Department of Molecular and Cellular Physiology, Hopkins Marine Station of Stanford University, Pacific Grove, California 93950 USA

ABSTRACT Properties of squid giant fiber lobe (GFL) Ca^{2+} channel deactivation (closing) were studied using whole-cell voltage clamp. Tail currents displayed biexponential decay, and fast and slow components of these tails exhibited similar external Ca^{2+}- and voltage-dependence. Both components also shared similar inactivation properties. Increasing duration pulses to strongly depolarizing potentials caused a substantial slowing of the rate of deactivation for the fast component, and also led to an apparent conversion of fast tail currents to slow without an increase in total tail amplitude. A five-state kinetic model that computed the closing of channels differentially populating two open states could simulate the kinetic characteristics of GFL Ca^{2+} pulse and tail currents over a wide voltage range. The kinetics of the proposed state transition was very similar to the time course of relief of ω-Agatoxin IVA Ca^{2+} channel block with long pulses. A similar model predicted that the relief of block could occur via faster toxin dissociation from the second open state. Thus, GFL Ca^{2+} channels possess a unique form of voltage-dependent gating modification, in which maintained prior depolarization leads to a significant delay to channel closure at negative potentials. At the nerve terminal, amplified Ca^{2+} signals generated by such a mechanism might alter synaptic responses to repetitive stimulation.

INTRODUCTION

Neuronal voltage-gated Ca^{2+} channels are responsible for providing the influx of Ca^{2+} ions necessary to evoke the release of neurotransmitter (Augustine et al., 1987). These channels are found in close proximity to sites of vesicle exocytosis (Smith et al., 1993), and with depolarization, Ca^{2+} channel opening leads to dramatic increases in local Ca^{2+} concentrations (Llinás et al., 1992). Despite this increased channel open probability, the driving force for Ca^{2+} ion entry is low at depolarizing potentials; upon membrane repolarization, a large amount of Ca^{2+} enters the neuron as channels close. The bolus of Ca^{2+} influx provided by such "tail currents" is likely responsible for timing of synaptic events in vivo (Llinás et al., 1981b).

In this study, I evaluated the deactivation (closing) properties of squid giant fiber lobe (GFL) Ca^{2+} channels by analyzing tail currents. Deactivation was observed to occur with a biexponential time course, which for Ca^{2+} channels expressed in some other cell types indicates the presence of two independent populations of Ca^{2+} channel (Matteson and Armstrong, 1986; Swandulla and Armstrong, 1988). In contrast, the experimental data in the present study were best explained by the presence of a single Ca^{2+} channel species with complex gating. The rate of channel closing was observed to slow substantially with increasing depolarization with no change in total Ca^{2+} conductance. This response to maintained depolarization is quite different from other reported instances of voltage-dependent modulation of Ca^{2+} channel gating (Hoshi and Smith, 1987; Pietrobon and Hess, 1990; Artalejo et al., 1991; Slesinger and Lansman, 1991; Nakayama and Brading, 1993, 1995; Kavalali and Plummer, 1994; Fleig and Penner, 1995). The voltage-dependent slowing of deactivation can be adequately described by a kinetic model that predicts the presence of two open states connected through a closed state. This model can further account for the state-dependent relief of Ca^{2+} channel block by ω-Agatoxin IVA (ω-Aga IVA), which occurs with similar kinetics.

METHODS

Isolation of GFL neurons from protease-treated squid (*Loligo opalescens*) stellate ganglia has been previously described (McFarlane and Gilly, 1996). In these experiments, neurons were cultured up to 5 days at 16–17°C in an L-15-based culture medium (Gibco, Grand Island, NY) supplemented with: 263 mM NaCl, 4.6 mM KCl, 49.5 mM $MgCl_2$, 4.5 mM $CaCl_2$, and 2 mM HEPES. L-Glutamine (2 mM final concentration), penicillin G (50 U/ml), and streptomycin (0.5 mg/ml) were added as a premixed stock solution (Irvine Scientific, Santa Ana, CA), and pH adjusted to 7.6.

Whole-cell recording was performed at 15–17°C using thick-walled borosilicate patch pipettes (7052, Garner Glass, Claremont, CA), which were fire-polished ($R_{pipette}$ = 0.25–0.40 MΩ) and filled with an internal solution that contained 451 mM tetramethylammonium (TMA)-aspartate, 25 mM TMA-F, 25 mM tetraethlyammonium (TEA)-chloride, 20 mM EGTA, 20 mM HEPES, and 4 mM MgATP. The external solution was composed of 480 mM TMA-Cl, 60 mM $CaCl_2$, 10 mM TEA-Cl, 10 mM HEPES, and 500 nM tetrodotoxin. Where indicated, external Ca^{2+} was lowered to 15 mM without magnesium replacement. All solutions were adjusted to pH = 7.6–7.7 and 990-1010 mOsmol. Control and test solutions for experiments using ω-Aga IVA (Pfizer Inc., New Groton, CT) contained 0.1 mg/ml lysozyme.

Calcium currents from the somata of GFL neurons without processes were acquired (50 kHz sampling rate for tail currents) from a patch-clamp amplifier with electronic capacitance compensation and were low-pass filtered using an eight-pole Bessel filter at 10 kHz. Series resistance (R_s) compensation (65 ± 4%) was always used during recording. Linear ionic and residual capacity currents were subtracted using a P/−4 method from

Received for publication 12 June 1996 and in final form 3 December 1996.
Address reprint requests to Dr. Matthew B. McFarlane, Hopkins Marine Station, Pacific Grove, CA 93950. Tel.: 408-655-6200; Fax: 408-375-0793.

0006-3495/97/04/1607/15 $2.00

the holding potential of −80 mV. The quality and speed of voltage clamp were assessed during the experiment by evaluating the characteristics of transients generated by −10 mV steps. Data were not analyzed from cells where the clamp time constant exceeded 60 μs (equivalent 90% rise time ~225 μs for a 200 mV voltage jump), or where errors in voltage control were >10 mV for large currents.

Data were analyzed using the IGOR Pro data analysis software for the Macintosh (WaveMetrics, Lake Oswego, OR), which uses the Levenberg-Marquardt algorithm for iterative curve fitting. Calcium tail currents were simultaneously fit to the sum of two exponential functions, and the time constants for fast (τ_{FAST}) and slow (τ_{SLOW}) tail components were generated from the fit. Amplitudes of fast (A_{FAST}) and slow (A_{SLOW}) components of the tail were calculated at the time of the peak of the total measured tail current (A_{TOT}). Comparison of A_{TOT} values to extrapolation of the double-exponential fit to $t = 0$ indicates that these measurements underestimate tail-current amplitude due to voltage-clamp delays. Most of the measurement errors associated with these large tail currents can be attributed to underestimation of the fast component, and for the slow component, only a small difference was observed between current amplitude obtained from fits at time 0 versus the time at peak of the tail currents (see comparison in legend to Fig. 4). The relatively uniform voltage-clamp conditions and calcium current levels for the data presented ensure that the amount of error was comparable between neurons.

Kinetic models used to simulate Ca^{2+} channel gating were based on conventional rate theory, and used independent forward and reverse rate constants to simultaneously solve first-order differential equations representing transitions between sequential closed and open states. Rates were assumed to change instantaneously with voltage and behave in a Markovian fashion. Specific channel distribution (dwell time) among these states was recalculated every 10 μs.

RESULTS

Experimental data

Currents through Ca^{2+} channels of cultured squid GFL neurons are shown in Fig. 1 *A* for a series of 25-ms voltage steps delivered in the presence of 15 mM (*closed circle*) and

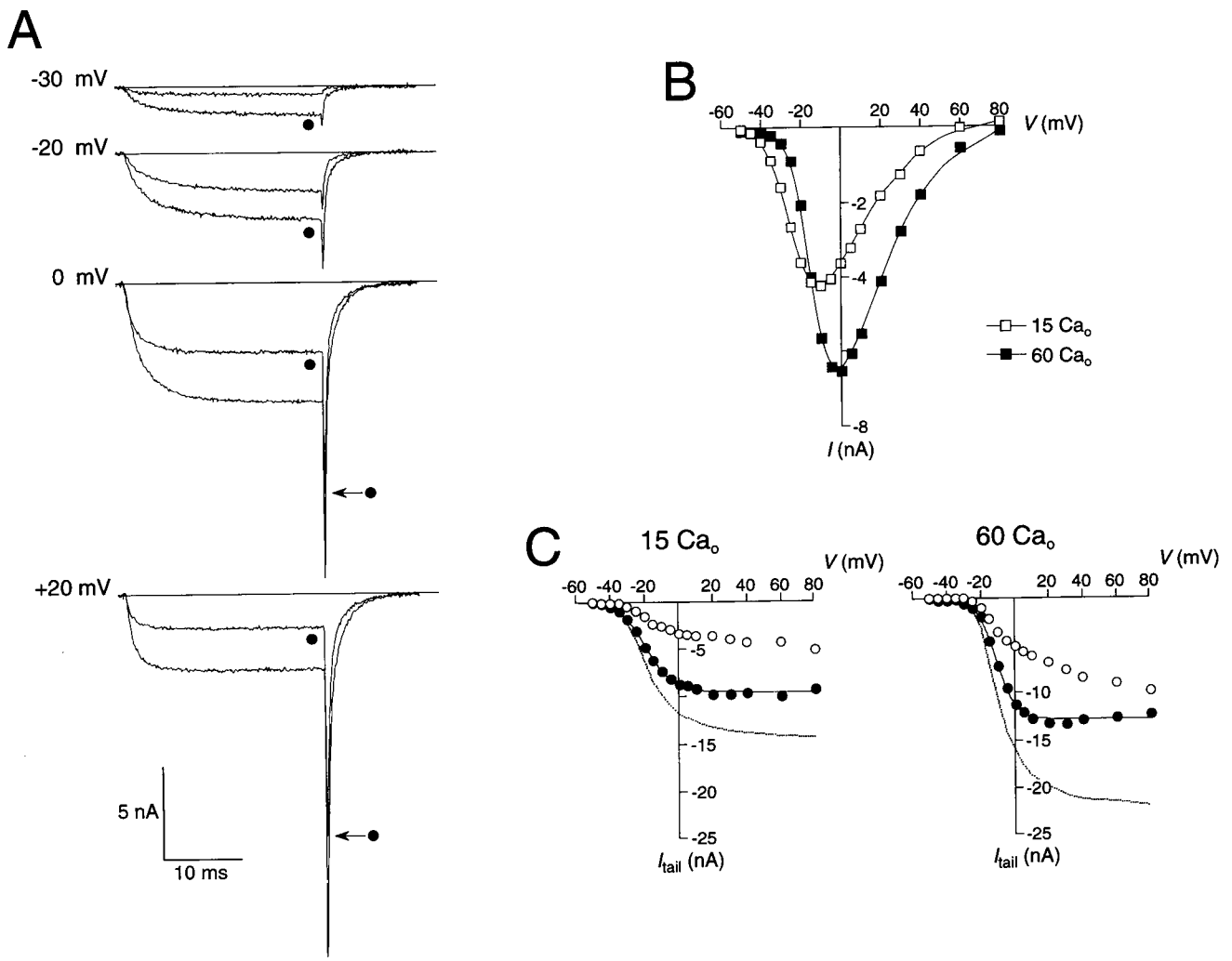

FIGURE 1 Fast and slow tail currents are carried by Ca^{2+} ions. (*A*), 25-ms step depolarization generates inward currents that are sensitive to external Ca^{2+} concentration. Traces are shown in the same neuron for pulses to the indicated potential in 15 mM Ca_o (*closed circles*) and normal (60 mM Ca_o) external solution. (*B*), Current-voltage relation at 25 ms for cell in (*A*) in 15 mM (*open squares*) versus 60 mM Ca_o (*closed squares*). (*C*) Tail current-voltage relations at −80 mV after 25-ms pulses in 15 mM (*left*) and 60 mM Ca_o. For each concentration, A_{TOT} (*stippled line*) is plotted together with A_{FAST} (*closed circles*) and A_{SLOW} (*open circles*) as a function of pulse voltage. The A_{FAST}-V curve in each case is fit with a single Boltzmann function, $I_{max}/(1 + \exp[(V_m - V_{1/2})/k])$. (15 Ca_o: k = 7.7 mV, $V_{1/2}$ = −19.0 mV, I_{max} = −9.5 nA; 60 Ca_o: k = 5.7 mV, $V_{1/2}$ = −11.2 mV, I_{max} = −12.85 nA) (cell 27g).

60 mM Ca^{2+} in the external solution. Lowering the extracellular Ca^{2+} concentration (Ca_o) shifts gating of Ca^{2+} (Zhou and Jones, 1995) and other channels (Hille, 1968) negatively along the voltage axis. Fig. 1 *A* demonstrates these effects in GFL neurons, as the macroscopic Ca^{2+} current ($I_{Ca^{2+}}$) is clearly larger at −30 and −20 mV in 15 mM versus 60 mM Ca_o, but at more positive potentials, currents are larger in 60 mM Ca_o. The current (25 ms)-voltage relations for 15 mM and 60 mM Ca_o are shown in Fig. 1 *B*. Both the threshold for channel activation and the peak of the $I_{Ca^{2+}}$-*V* curve are shifted by ~−10 mV as Ca_o is lowered, and as expected, the amplitude of the peak is diminished as the permeant ion concentration is lowered.

The effects of lowering Ca_o can also be observed in the amplitude of tail currents at −80 mV (Fig. 1 *A*), as tails behave similarly to the amplitude of currents during the pulse. Previous studies on GFL neurons have identified two components of these tail currents (Lláno and Bookman, 1986; McFarlane and Gilly, 1996). The Ca_o-dependence of both tail current components is demonstrated in Fig. 1 *C*, where the total tail amplitude (A_{TOT}, *dashed line*) is plotted along with fast (A_{FAST}, *closed circles*) and slow (A_{SLOW}, *open circles*) components as a function of activation voltage for 15 mM (*left*) and 60 mM Ca_o. A_{FAST} values are well-fitted with a single Boltzmann function (*solid curve*), and I_{max} derived from this fit at positive voltages increases in high Ca_o. A_{SLOW} values could not be similarly fitted with a Boltzmann because no saturation is observed for this pulse duration (see also below). Like A_{FAST}, A_{SLOW} values increase in high Ca_o, and the overall shape of the relationship is preserved in 60 mM Ca_o. In addition, both components exhibit a similar magnitude positive voltage shift associated with raising Ca_o. In a similar experiment, complete replacement of external calcium with barium led to a parallel increase in the permeability of fast and slow tails (data not shown). These observations only indicate that both fast and slow components of the tail current result from the closing of Ca^{2+} channels.

Fast and slow tail currents contributed proportionally to the total instantaneous current-voltage relationship of Ca^{2+} channels. Typical tail currents recorded at a range of voltages from −140 to +60 mV following an activating pulse to +60 mV for 10 ms are shown in Fig. 2 *A*. Fast and slow tail current components can be resolved at voltages ≤−40 mV. To evaluate the behavior of Ca^{2+} tail currents in neurons with variable levels of Ca^{2+} channel expression, mean A_{TOT} values (n = 7) were normalized (A_{TOT} at −140 mV = 1) and plotted along with mean fractional A_{FAST} and A_{SLOW} values as a function of tail voltage (Fig. 2 *B*). Fast and slow Ca^{2+} tail currents have been recorded from other molluscan neuronal somata (Byerly and Hagiwara, 1982; Brown et al., 1983; Eckert and Ewald, 1983), and in some cases, the slow component has been reported to saturate at negative voltages. This saturation is not observed for GFL Ca^{2+} channels. The time constants of fast (τ_{FAST}) and slow (τ_{SLOW}) components show a similar voltage-dependence (Fig. 2 *C*), and both τ_{FAST} and τ_{SLOW} increase sharply at voltages near the threshold for channel activation. Such similar voltage-dependency of fast and slow tail current components is quite different from instances where multiple families of Ca^{2+} channel are coexpressed in a given cell, as in the case of L- and T-type Ca^{2+} channels in neuroendo-

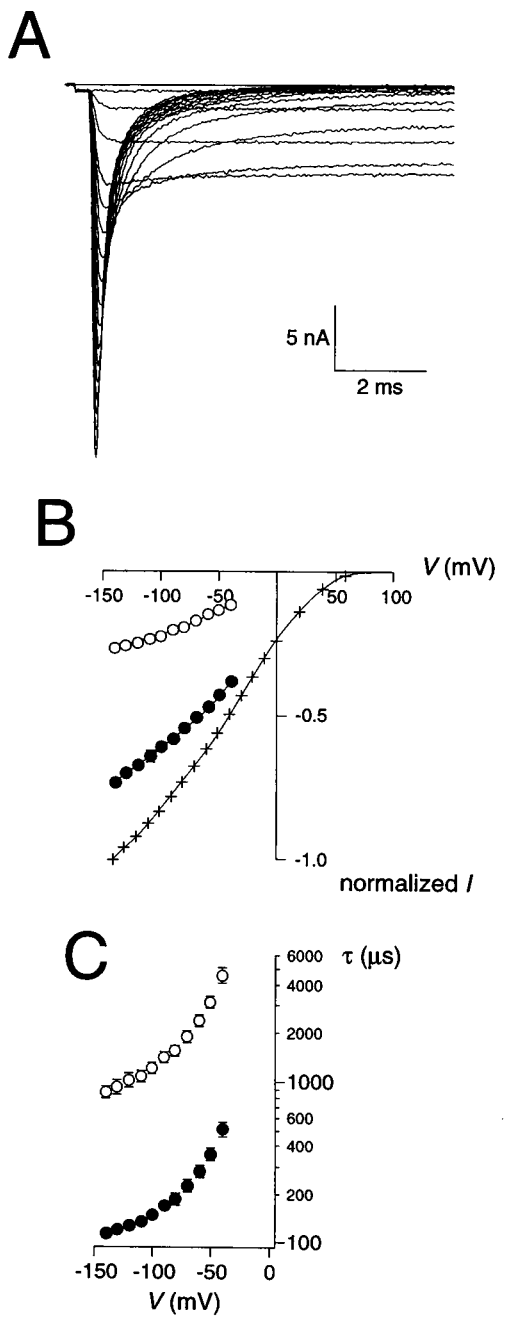

FIGURE 2 Instantaneous $I_{Ca^{2+}}$-*V* curves for fast and slow tail components of Ca^{2+} tail current. (*A*) Tail currents obtained at various potentials between −140 and +60 mV after a 10-ms activating pulse to +60 mV (cell 24e). (*B*) Mean (±SEM, n = 7) normalized (versus tail at −140 mV) instantaneous $I_{Ca^{2+}}$-*V* relations for total tail current (+). Mean fractional A_{FAST} (*closed circles*) and A_{SLOW} (*open circles*) values are shown for the potentials where tail currents were most reliably fit (−140 to −40 mV). (*C*) Mean time constants for relaxation of fast (*closed circles*, τ_{FAST}) and slow (*open circles*, τ_{SLOW}) tail currents.

crine cells (Matteson and Armstrong, 1986). In this case, different closing properties are exhibited by fast and slow components corresponding to high- and low-voltage-activated Ca^{2+} channels.

Differences in the steady-state inactivation properties of fast and slow components were assessed in Fig. 3 by testing the sensitivity to various holding potentials. Cells were held at a particular potential 1–5 min before recording test pulses, and the effects of increasing holding potential were only partially reversible. In this experiment, tail currents were measured at −80 mV after a 5-ms activating pulse to +60 mV. Amplitudes of both fast (*closed circles*) and slow (*open circles*) components were measured from seven GFL neurons, and the mean normalized values are shown plotted as a function of holding potential (Fig. 3 *A*). Both A_{FAST} and A_{SLOW} begin to decrease for potentials >-50 mV, and then decrease by the same fraction for more positive voltages. Both sets of data are shown fit with similar single Boltzmann functions (fit parameters in legend to Fig. 3), and the large overlap between the two components indicates that both fast and slow tail currents share a similar sensitivity to holding potential. This finding further suggests that the Ca^{2+} channels underlying fast and slow tail currents show analogous voltage-dependent properties.

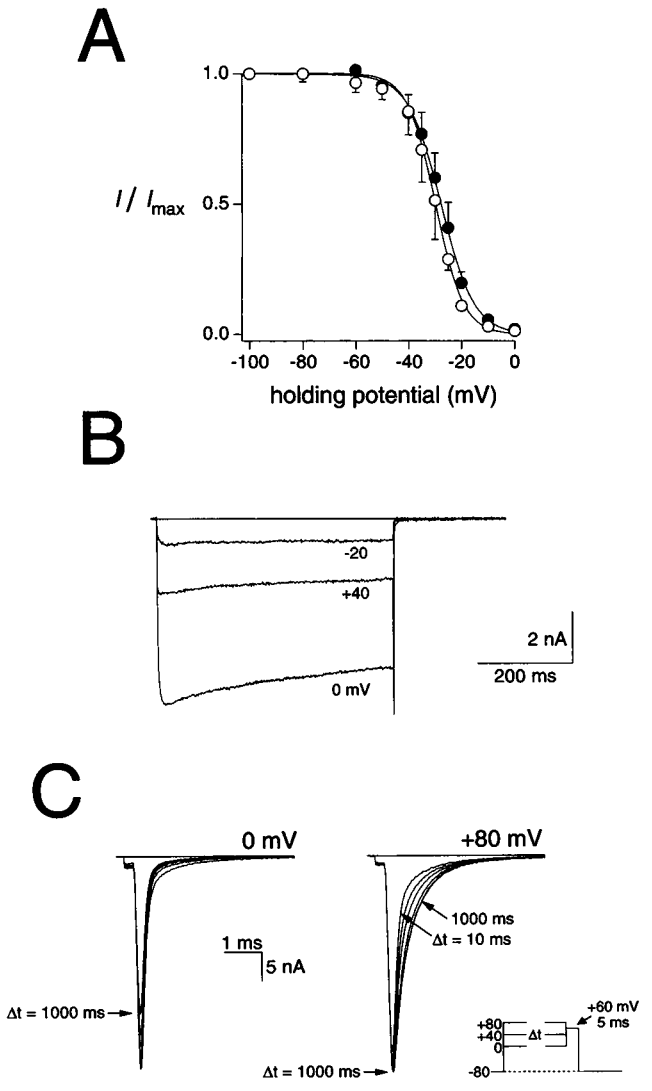

FIGURE 3 Inactivation characteristics of GFL $I_{Ca^{2+}}$. (*A*) Tail currents were recorded at −80 mV after a 5-ms pulse to +60 mV at various holding potentials. Amplitudes of individual tail current components were determined and were normalized to their peak value to yield I/I_{max}. Mean (±SEM, $n = 5$) I/I_{max} values are shown for A_{FAST} (*closed circles*) and A_{SLOW} (*open circles*) plotted as a function of the holding potential. These values are shown with the best fits of single Boltzmann functions (A_{FAST}: $V_{1/2} = -27.7$ mV, $k = 3.9$ mV; A_{SLOW}: $V_{1/2} = -29.7$ mV, $k = 4.7$ mV). (*B*) 500-ms pulses to the potential indicated on the traces (cell 16b). (*C*) A standard prepulse protocol (*inset*) was followed by a 5-ms test pulse to +60 mV, after which tail currents were recorded at −80 mV. Left panel, tail currents after increasing duration (Δt = 10, 50, 100, 500, and 1000) prepulses to 0 mV (1000-ms prepulse marked with *arrow*). Right panel, tail currents after increasing duration prepulses to +80 mV (cell 16b)

While inactivation of GFL $I_{Ca^{2+}}$ can be produced quite effectively by increasing holding potential, the rate of inactivation is very slow during long pulses (Fig. 3 *B*). Inactivation is most prominent for potentials near the peak of the $I_{Ca^{2+}}$-V relationship (~0 mV), and based on the time course of decay observed for most GFL neurons, estimates for half-times of inactivation at 0 mV range from 1.5 to 2.5 s. A lesser degree of inactivation is observed for more positive or more negative voltages. Very slow inactivation can also be studied for fast and slow tail currents using a standard prepulse protocol (Fig. 3 *C*). Increasing duration (Δt) prepulses to 0 mV produce an increasing decay in both fast and slow tail current components (*left panel*), and the magnitude of the decrease in the total tail current is similar to that observed for currents during long pulses. For the same neuron, prepulses to +80 mV caused very little change in total tail current amplitude (*right panel*).

The more significant difference observed for increasing duration prepulses to strongly depolarizing potentials, however, is that tail current kinetics slow considerably. Inspection of the tail currents for prepulses to +80 mV (Fig. 3 *C*) show both an increase in the amplitude of the slow tail current component as well as a significant slowing of the time course of the fast component (compare Δt = 10 vs. 1000 ms). These changes are observed to a far lesser extent for prepulse depolarizations to +40 mV (not shown), and not at all for prepulses to 0 mV (Fig. 3 *C*, *left*).

This same effect is observed for pulses to +60 mV, where the amplitude of the slow component values continue to increase without an increase in total tail current amplitude, suggesting that no additional channels have been opened during the long pulse. This result is shown in Fig. 4 *A*, which displays tail current traces at −80 mV for increasing pulse durations to +60 mV (Δt). Both the increase in the slow component and the slowing of the fast component appear to saturate between Δt = 500 and 1000 ms. Fig. 4 *B* illustrates the fast component of tail current records following subtraction of slow components from the parent records in Fig. 4 *A*. In addition to the amplitude decrease accompanying the increase in A_{SLOW}, τ_{FAST} increased in this neuron from 190 μs (Δt = 5 ms) to 346 μs (Δt = 500 ms),

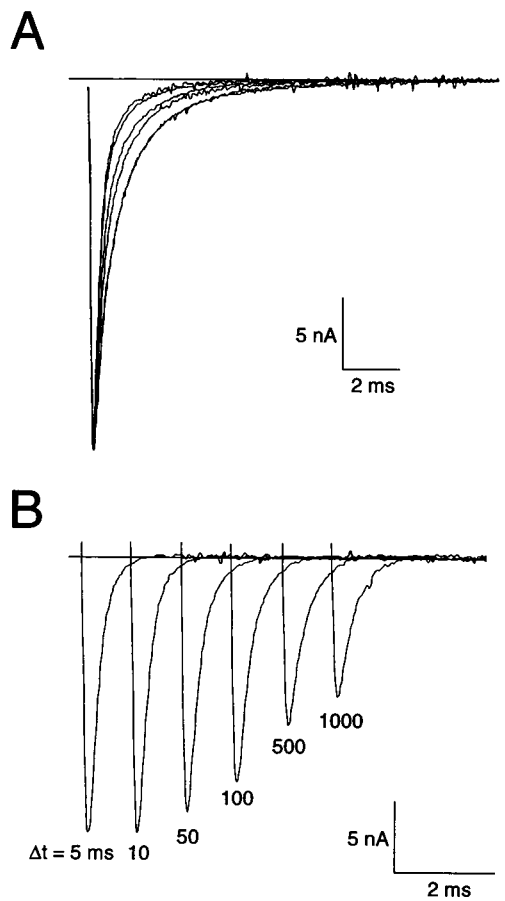

FIGURE 4 Increasing length of depolarization changes the relative contribution of fast and slow components of tail currents. (*A*) Tail currents generated at −80 mV after depolarization to +60 mV for durations between 5 and 1000 ms. (*B*) Fast component of tail currents from (*A*) are shown in isolation. The pulse length (Δt) is indicated below the trace. (*C*) Values for A_{FAST} (*closed circles*), A_{SLOW} (*open circles*), and A_{TOT} (+) are plotted as a function of depolarization time to +60 mV. For a 140-mV voltage jump in this neuron (50 kHz sampling rates), A_{TOT} and A_{FAST} values were underestimated by 13.8 ± 1.6% and 17.8 ± 1.8%, respectively. Much less error was associated with determination of A_{SLOW} (4.2 ± 0.4%, n = 6 for each). A_{FAST} values are fitted with a single exponential (τ = 242 ms), and A_{SLOW} values are similarly fitted (τ = 128 ms) (cell 25b).

and an approximate twofold increase in τ_{FAST} was observed for all neurons. A much smaller effect on the kinetics of the slow tail current was usually seen, and for this cell τ_{SLOW} increased from 1.43 ms (Δt = 5 ms) to 1.59 ms (Δt = 500 ms). A_{TOT} (+), A_{FAST} (*closed circles*), and A_{SLOW} (*open circles*) values calculated at the time of the peak of the tail current for this experiment are plotted as a function of depolarization time (Δt) in Fig. 4 *C*. Constancy of total tail current amplitude apparently reflects a complementary balance between changes in A_{FAST} and A_{SLOW}.

Slow deactivation after long pulses was present at all negative voltages. Fig. 5 *A* shows tail current traces following an activating pulse to +60 mV for Δt = 5 and 500 ms (*closed circles*). In each case, the slow component of tail currents was small for Δt = 5 ms and increased for Δt = 500 ms. This effect is most pronounced in the voltage range immediately negative to the threshold for activation (e.g., −40 to −80 mV). There was also a significant effect on the deactivation kinetics of the fast component, which was measurably slower at these voltages (see Fig. 4). The instantaneous $I_{Ca^{2+}}$-V relationship for Δt = 5 (*small open circles*) and 500 ms (*large closed circles*) is plotted in Fig. 5 *B*. Even though the amplitude of slow tail currents increased for Δt = 500 ms, the $I_{Ca^{2+}}$-V curves for both durations are indistinguishable. This observation indicates that maintained depolarization slowed channel deactivation

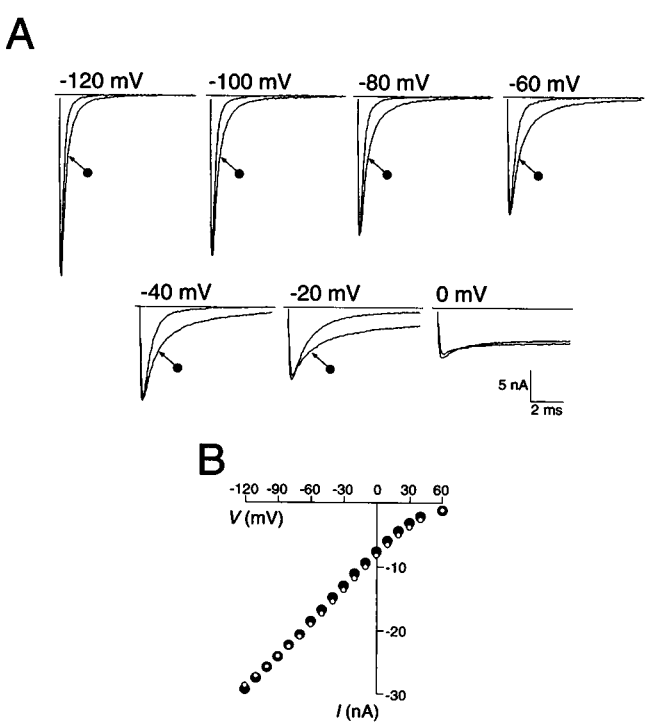

FIGURE 5 Extended depolarization causes slower deactivation at negative voltages. (*A*) Tail current traces were recorded at the indicated potential after pulses to +60 mV for Δt = 5 and 500 ms (*closed circle*). (*B*) Instantaneous current-voltage relationship for Δt = 5 (*open circle*) and 500 ms (*closed circle*). Peak amplitudes of tail currents are plotted (cell 27d).

without affecting the number of open channels at the end of the pulse.

Three explanations have been offered to explain the presence of biexponential Ca^{2+} tail currents in a number of different preparations. 1) Ca^{2+} channels may be present together with channels that generate unrelated currents, such as proton currents in snail neurons (Byerly and Hagiwara, 1982). 2) Two independent populations of Ca^{2+} channel may be present in the same cell (Matteson and Armstrong, 1986; Swandulla and Armstrong, 1988). 3) A single type of Ca^{2+} channel with a complex gating mechanism could generate fast and slow tail currents (Brown et al., 1983; Taylor, 1988).

Because fast and slow tail currents share the same Ca_o-dependence and divalent cation selectivity, it is likely that both fast and slow tail currents arise from Ca^{2+} channels. Thus, explanation 1) is unlikely to be the case. Distinguishing between explanations 2) and 3) is more complicated because conflicting reports exist regarding the behavior of fast and slow Ca^{2+} tail currents in GFL neurons. The results of the previous section showed that the voltage-dependence of inactivation is very similar between the two components. However, Lláno and Bookman (1986) reported that slow (but not fast) tail currents inactivated over long depolarization times and that slow tails activate at more negative voltages than do fast tails. These authors proposed the existence of two distinct Ca^{2+} channel types, but their slow tail currents may have been largely due to voltage-dependent K^+ channels, because 10 mM external K^+ was present and no agents were used to block inward K^+ tail currents. Following the idea of two distinct channel types, Chow (1991) used a Hodgkin-Huxley m^2-type kinetic scheme to account for macroscopic $I_{Ca^{2+}}$ activation and deactivation, and could disregard the presence of the slow tail current in his modeling of Ca^{2+} channel block by cadmium ions. Thus, neither of these previous studies provides strong support for the explanation that independently operating Ca^{2+} channel populations generate fast and slow tails 2), and they certainly do not disprove explanation 3), in which a single population of Ca^{2+} channel with two distinct closing rates generates fast and slow tails.

However, the properties of biexponential Ca^{2+} tail currents after conditioning depolarization offer strong evidence in support of explanation 3). The increase in the amplitude of the slow component with increasing pulse length occurs together with an equivalent decrease in the fast component, such that total the total tail current (and presumably the number of channels open at the end of the current pulse) stays relatively constant. For explanation 2) to be sufficient to explain these data, the slow increase in "A_{SLOW} channel" activation would have to be coincidentally matched by inactivation of "A_{FAST} channels." Explanation 3) offers a more plausible scenario: the apparently complementary behavior of fast and slow tail current components results from the complex deactivation properties of a single population of noninactivating Ca^{2+} channels.

Kinetic Modeling

The gating of GFL Ca^{2+} channels was further investigated by testing the behavior of a number of kinetic models that represented the operation of a single-channel population. The main goal was to determine whether a single kinetic scheme could predict the general characteristics observed for GFL Ca^{2+} channels after increasing duration depolarization. The results presented in the previous section suggested that GFL Ca^{2+} channels undergo a slow voltage-dependent state transition, which is observable as changes in deactivation kinetics. This being the case, four kinetic models were tested for their ability to account for the change-over of tail currents from predominantly fast (after short depolarizations) to slow (after long depolarizations) given a single set of rate constants for a particular voltage. All models tested have two sequential closed states in the main activation pathway, and transitions between these states were assumed to follow Hodgkin-Huxley m^2 kinetics. This approach has been previously utilized to describe activation/deactivation of GFL $I_{Ca^{2+}}$, and gives reasonable fits for data obtained under these experimental conditions as well (Chow, 1991; see also below). A useful model should pass the following three tests of adequacy:

Test A

Changing distribution of channels among states at a particular activating voltage should produce changes in the kinetics of macroscopic $I_{Ca^{2+}}$ deactivation for a single set of rate constants at a negative closing voltage.

Test B

Appropriate channel redistribution over time at depolarizing potentials (e.g., +60 mV) must be accomplished using a single set of rate constants.

Test C

Some or all of these rate constants should change smoothly, (e.g., exponentially) with voltage, and macroscopic $I_{Ca^{2+}}$ activation and deactivation kinetics should be predictable over a wide voltage range.

Biexponential Ca^{2+} tail currents can be described by channel closure to two sequential closed states from a single open state (Brown et al., 1983; Taylor, 1988). This may be the case if the forward rate constants for opening are appreciable at a particular voltage. For voltages sufficiently below activation threshold, these forward rates should be small, and −80 mV is probably negative enough to ensure that forward (opening) rate constants are near zero. Under these conditions, multi-exponential deactivation is likely to result from transitions to closed states other than those along the activation pathway. Closing along each of these pathways would generate an identifiable exponential component

to macroscopic tail currents only if these transitions occur with significantly different rates (Armstrong and Matteson, 1984). For example, Hoshi et al. (1994) observed a tri-exponential deactivation time course of *Shaker* potassium channels, which suggested the presence of two closing pathways in addition to the closed state along the activation pathway.

Model 1 tests this type of gating scheme, which permits transition into and out of an additional closed state, C^*.

$$C_2 \leftrightarrow C_1 \leftrightarrow O_1 \leftrightarrow C^*$$

Model 1

Open channels may close to either C_1 or C^*, and these two transitions ($O \rightarrow C_1$ or $O \rightarrow C^*$) account for the fast and slow deactivation components, with τ_{FAST} and τ_{SLOW} reflecting the overall rate of channel closing. Model 1 can predict biexponential tail currents. The model is inadequate, however, because the rate constants must change over time to account for shifts in the relative amplitudes of fast and slow components, and thus fails adequacy test A.

Biexponential deactivation may also indicate the presence of multiple open states, and the majority of the slowly deactivating component could be due to transition between the two open states with equal unitary conductances. For example, in model 2, the fast Ca^{2+} tail current component that dominates for short pulses results from rapid channel closings from O_1 ($O_1 \rightarrow C_1$; $\tau_{FAST} = 1/k_{O_1 \rightarrow C_1}$). Slower deactivation is generated from channels in O_2 that must pass to O_1 relatively slowly, because of slow $O_1 \leftrightarrow O_2$ transitions, before they ultimately close from O_1. Similarly, model 3 presumes that channels in O_2 may either pass directly to a closed state along an independent closing pathway (C_1^*) or traverse to O_1, from which closure to C_1 is highly preferred.

$$C_2 \leftrightarrow C_1 \leftrightarrow O_1 \leftrightarrow O_2$$

Model 2

$$\begin{array}{c} C_2 \leftrightarrow C_1 \leftrightarrow O_1 \\ \updownarrow \\ C_1^* \leftrightarrow O_2 \end{array}$$

Model 3

Acceptability of two open state models was evaluated in the following way. Characteristics of tail currents were observed for a single set of rate constants (developed for tail currents at −80 mV) as channels were placed either in O_1 or O_2, such that total occupancy of $O_1 + O_2$ was constant. Given that total tail amplitude does not change, it was assumed that increasing the fraction of channels in O_2 (fO_2) would be accompanied by a complementary decrease in the fraction of channels in O_1 (fO_1), such that $fO_2 + fO_1 = 1$. Another assumption was that the voltage- and time-dependent transition of tails from fast to slow during a depolarizing pulse was a consequence of an open state (i.e., $O_1 \rightarrow O_2$) transition. This $O_1 \rightarrow O_2$ transition must produce both the correct changes in A_{FAST} and A_{SLOW}, and a twofold increase in τ_{FAST} but not τ_{SLOW}. Thus, a useful model would approximate this behavior in a manner dependent only on the population of O_2 vs. O_1.

The amplitude of the slow tail current component calculated by models 2 and 3 mirrors the fO_2 value. If no channels are in O_2, the tails are single-exponential and fast. Conversely, if all channels are in O_2, tail currents are single-exponential and slow. Biexponential tail currents were generated by combinations of fO_1 and fO_2, but the individual fast and slow rates did not change, and therefore no combination of rate constants predicts an increase in τ_{FAST} as fO_2 is increased. Neither model 2 nor model 3 was able to simulate GFL Ca^{2+} tail currents, as the calculated biexponential tail currents were always linear combinations of fast and slow exponentials with the same rates. Consequently, models 2 and 3 fail adequacy test A, and thus, directly communicating open states are unlikely to account for the effects of extended depolarization.

In light of this finding, an alternative way of interpreting the slowing of τ_{FAST} is necessary. Fast and slow tail currents are visible after brief pulses, and these two exponential components must reflect the presence of at least three channel states (for n components, number of states = $n + 1$; Armstrong and Matteson, 1984; Hoshi et al., 1994). The observed variation in the fast time constant for long, strong depolarization indicates the presence of a third exponential component in the system. The decay time constant of this component is probably in between the fast and slow time constants recorded after short pulses (but closer to the fast). Had this intermediate exponential component been much slower than both fast and slow tails, one would expect that tail currents would follow a tri-exponential time course, as has been described for Ca^{2+} channels in *Helix* neurons (voltage-dependent appearance of $\tau_{VERY\ SLOW}$; Brown et al., 1983). Based on this reasoning, the slowing of the fast tail provides suggestive evidence for a third exponential component that becomes more prominent with increasing pulse duration.

To account for these observations, (at least) four channel states are required in the gating model. The assumption was made that for these noninactivating channels the two open states are likely to have the same unitary conductance. Given this condition, model 2 cannot account for the third exponential because transitions between O_1 and O_2 are not observable, and model 3 only partially compensates for this deficiency by allowing closures directly from O_2, but the extent to which these closures can account for an overall slowing of τ_{FAST} is limited.

The idea was tested that channels enter O_2 from O_1 by passing through a closed-"inactive" (CI) state, as in model 4. The inclusion of CI makes O_2 kinetically distinct from O_1 because channels leaving O_2 must close before reopening to either O_1 or O_2. These reopenings are therefore postulated to account for the appearance of the intermediate

$$C_2 \leftrightarrow C_1 \leftrightarrow O_1 \leftrightarrow CI \leftrightarrow O_2$$

Model 4

TABLE 1 Rate constants used for model 4

Voltage (mV)	$k_{C_2 \to C_1}$	$k_{C_1 \to C_2}$	$k_{C_1 \to O_1}$	$k_{O_1 \to C_1}$	$k_{O_1 \to CI}$	$k_{CI \to O_1}$	$k_{CI \to O_2}$	$k_{O_2 \to CI}$
−80	0.020	2.100	0.010	4.20	0.0010	0.530	0.10	1.16
0	0.680	0.225	0.340	0.45	0.0032	0.204	0.68	0.21
+20	1.340	0.140	0.670	0.28	0.0044	0.184	1.10	0.13
+40	2.480	0.075	1.240	0.15	0.0058	0.129	1.80	0.09
+60	4.840	0.044	2.420	0.09	0.0080	0.100	3.00	0.06
+80	9.200	0.025	4.600	0.05	0.0106	0.080	4.80	0.04

Rate constants were determined for data obtained from cell 27d (traces in Fig. 5 and 6). Rates were assumed to change exponentially with voltage. All rates expressed in ms^{-1}.

exponential component with extended depolarization. Also, channels that accumulate in O_2 indirectly contribute the increase in A_{SLOW}, as channels must pass through CI and O_1 to fully close.

Model 4 is presumed to operate in the following way. For short-duration pulses, channels are predominantly in O_1. After repolarization, channels in O_1 can close to either C_1 or CI. Closure to C_1 is presumed to account for the fast component of the tail, because at highly negative potentials, channels in C_1 would continue along the closing pathway to C_2. On the other hand, closure to CI is assumed to account for the slow component, because channels in CI need to pass through O_1 (and reopen) to close to C_1. This is similar to "bursting"-type models, where multiple closed or inactive states associated with a single open state produce biexponential channel closing (Forti and Pietrobon, 1993; Hoshi et al., 1994). This model predicts that a slow tail component is present even after short pulses, which is observed experimentally.

For longer pulses, channels are presumed to gradually accumulate in O_2. Channel closure from O_2 to CI is proposed to account for an intermediate component, and increasing the fraction of channels in O_2 would lead to the apparent slowing of τ_{FAST}. Channels in CI can reopen to O_1, or reopen to O_2, which would further slow deactivation.

Five steps were used to determine the rate constants for model 4:

1) $C_2 \leftrightarrow C_1$ and $C_1 \leftrightarrow O_1$ transitions were assumed to follow m^2 kinetics (see above), thus $k_{C_2 \to C_1} = 2 \times k_{C_1 \to O_1}$, and $k_{O_1 \to C_1} = 2 \times k_{C_1 \to C_2}$. Values for $k_{C_1 \to C_2}$ (and $k_{O_1 \to C_1}$) and $k_{CI \to O_1}$ were estimated from tail currents recorded at −80 mV.
2) The fO_2 analysis (see models 2 and 3) was used to determine whether tail current kinetics could change for the same set of rate constants. This analysis yielded values for $k_{O_1 \to CI}/k_{CI \to O_1}$ and $k_{CI \to O_2}/k_{O_2 \to CI}$.

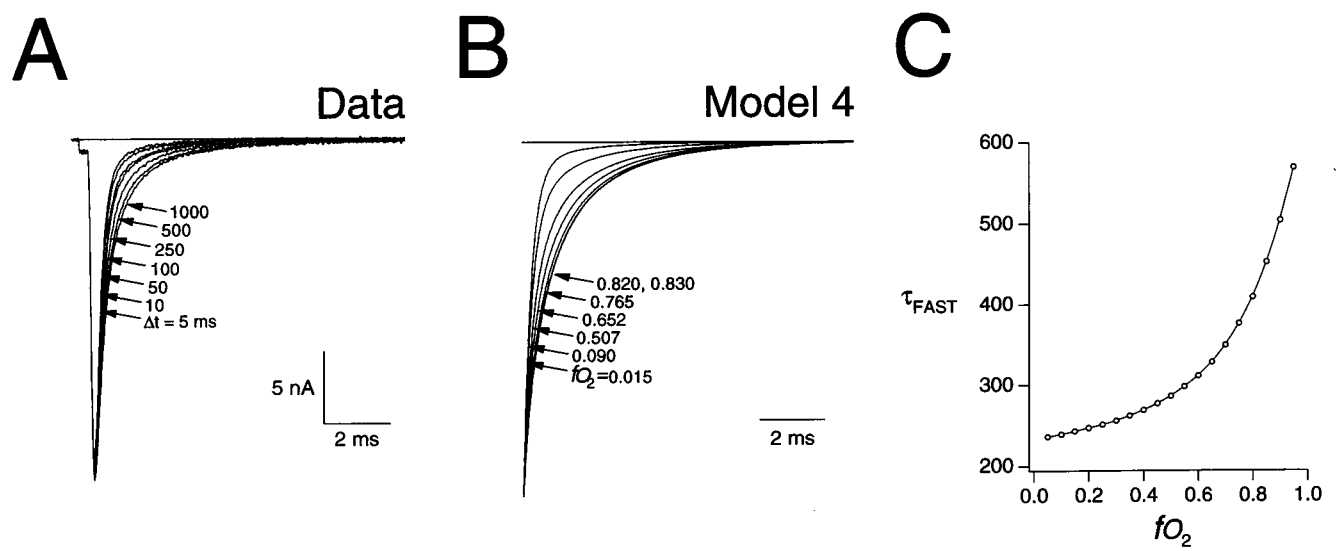

FIGURE 6 Comparison of experimental data to tail currents generated by model 4. (*A*) Tail currents were recorded at −80 mV after pulses to +60 mV for the indicated duration (Δt). The last 0.2 ms of current during the pulse are shown along with the tail (cell 27d). (*B*) Tail currents calculated from model 4 using the indicated fO_2 (with $fO_1 = 1 - fO_2$) value as an initial condition for each trace (initial values for C_2, C_1, and CI were 0). (*C*) Values for τ_{FAST} obtained from double exponential fits to modeled traces, plotted as a function of fO_2.

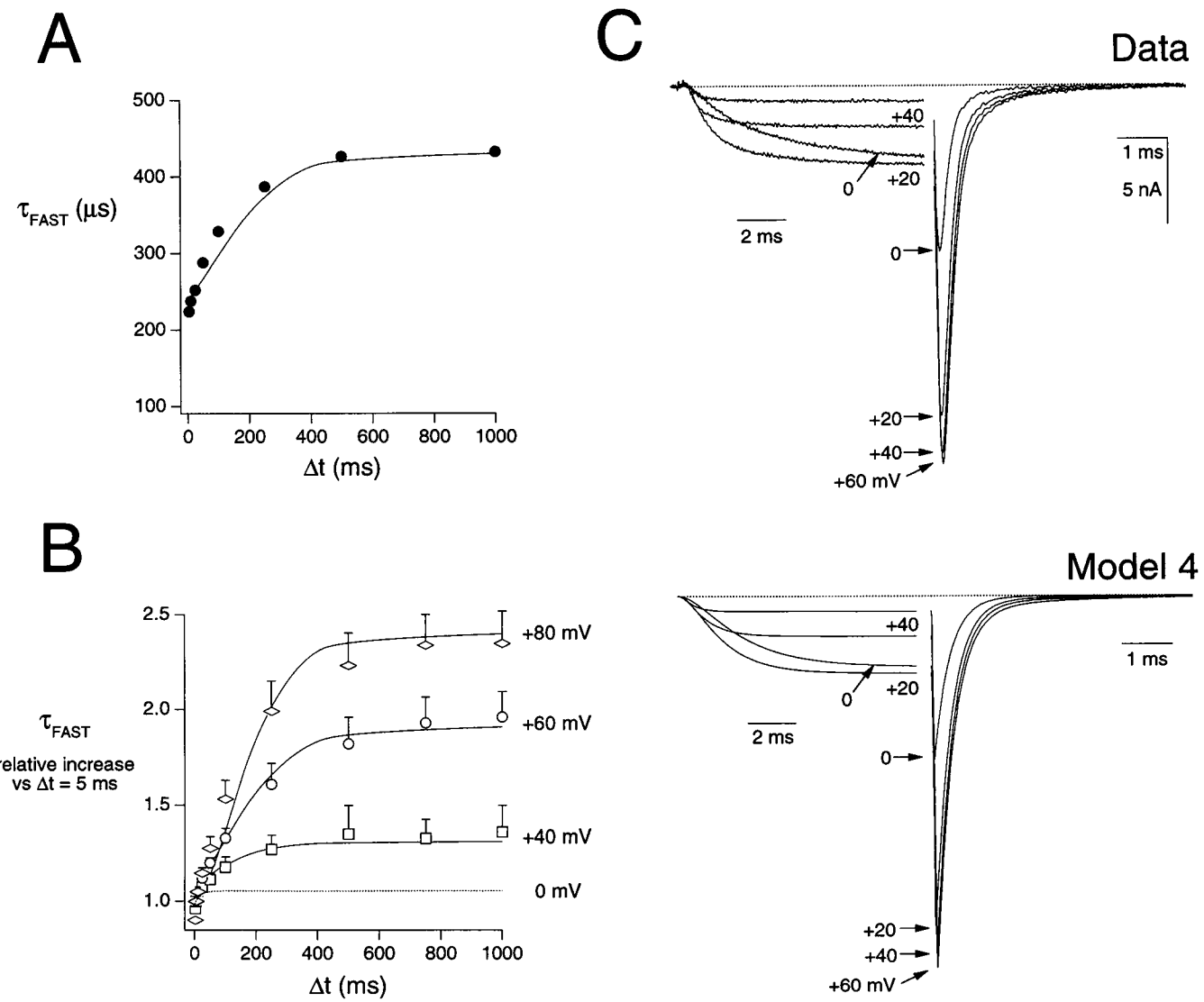

FIGURE 7 Properties of model 4. (*A*) Model 4 accounts for the time-dependent slowing of deactivation kinetics after pulses to +60 mV. τ_{FAST} values (*closed circles*) were obtained from Ca^{2+} tail currents at −80 mV after pulses to +60 mV for Δt duration. Model 4 was run at +60 mV for various Δt assuming all channels were initially in state C_2. The resulting distribution of channels among the five states was used as an initial condition to run the model at −80 mV. τ_{FAST} values were obtained from these tail currents (*smooth curve*). (*B*) Voltage-dependence of τ_{FAST} slowing can be described by the voltage-dependence of model 4 rate constants. Mean (±SEM) relative increase in τ_{FAST} for a given Δt are plotted for depolarization to +40 mV (*squares*, $n = 4$), +60 mV (*circles*, $n = 6$), and +80 mV (*diamonds*, $n = 7$). These values are shown along with the calculations of model 4 for the same Δt using rates shown in Table 1 (*curves*). The calculations of the model for 0 mV are also shown (*dashed line*). (*C*) GFL Ca^{2+} channel activation and deactivation kinetics are accurately described by model 4. The upper set of traces represents currents obtained during (*left*) and after (at −80 mV, *right*) 10-ms pulses to the indicated potential. Sampling rate in both cases was 50 kHz (cell 27d). The lower set of traces was simulated by model 4. Pulse currents were obtained assuming all channels were in C_2 at rest. A 0.4-ms delay after the start of the pulse was inserted, and the transient outward current observed in the experimental data was not modeled. Tail currents were calculated at −80 mV using the final distribution of channels among the five states obtained after the 10-ms pulse. Scaling factors were derived from the instantaneous $I_{Ca^{2+}}$-V relationship and were −28.0, −11.5, −6.65, and −2.65 nA for −80, 0, +20, and +40 mV, respectively.

3) Short pulses to intermediate voltages (−20 to +20 mV) were used to determine $k_{C_1 \rightarrow O_1}$ ($k_{C_2 \rightarrow C_1}$).
4) Values for $k_{O_1 \rightarrow CI}$ and $k_{CI \rightarrow O_2}$ were determined for +60 mV for increasing Δt in order to establish appropriate mixtures of O_1 and O_2.
5) All other rates at all other voltages were determined by assuming that rates change exponentially as a function of voltage (Table 1).

Fig. 6 *A* shows Ca^{2+} tail currents recorded at −80 mV in a GFL neuron after pulses of Δt duration to +60 mV. These currents are shown compared with characteristics of tail currents simulated by model 4 (Fig. 6 *B*) using fractional O_2 values indicated on the traces. These parameters were determined for modeled tail currents in the same fashion as for experimentally obtained tail currents. The model predicts tail current slowing when more channels are initially placed

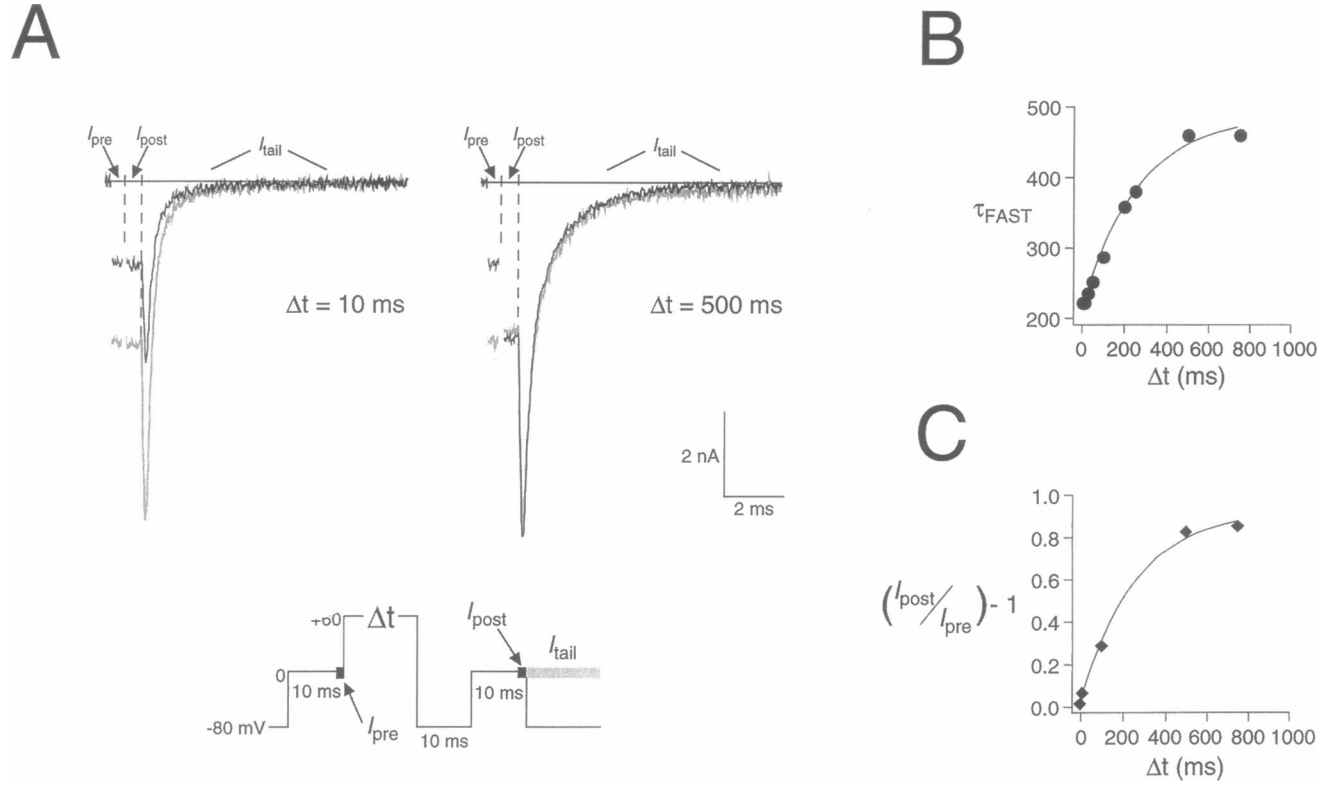

FIGURE 8 Relief of ω-Aga IVA block of GFL $I_{Ca^{2+}}$ is temporally correlated with the gating transition at +60 mV. (*A*) Effects of strong depolarization on Ca^{2+} currents. Two test pulses (0 mV, 10 ms) were separated by a variable duration step to +60 mV (*inset*). The second pulse was obtained after a 10-ms step to −80 mV to allow channels to close. $I_{Ca^{2+}}$ was evaluated at the final 0.5 ms of the test pulse before (I_{pre}) and following (I_{post}) the depolarizing pulse. Ca^{2+} tail currents (I_{tail}) were then recorded at −80 mV after the second test pulse. Pulse patterns were run in the absence (*gray traces*) and presence (*black traces*) of 500 nM ω-Aga IVA for Δt = 10 ms (*left*), and 500 ms (*right*). (*B*) τ_{FAST} values calculated in the absence of ω-Aga IVA plotted as a function of pulse duration to +60 mV (Δt). Values are shown fitted with a single exponential (τ = 264 ms). (*C*) Relief of ω-Aga IVA block was quantified using the equation (I_{post}/I_{pre}) − 1 following the same pulse protocol described in (*A*). Values obtained are plotted as a function of Δt and are also fitted with a single exponential (τ = 257 ms) (cell 28d).

in O_2, and this slowing is observed as an increase in both A_{SLOW} and τ_{FAST}. For these rate constants, increasing fO_2 from 0.2 to 0.8 led to a 1.66-fold increase in τ_{FAST} (from 247 to 409 μs), and a 3.4-fold increase in A_{SLOW} (from 0.135 to 0.460 μs). Over the same fO_2 range, τ_{SLOW} increased by 10.4% (1602–1768 μs). This shift in τ_{FAST} is plotted as a function of fO_2 in Fig. 6 *C*. τ_{FAST} values increase slightly but steadily for fO_2 values < 0.6, but increase more rapidly for $fO_2 > 0.6$. A_{SLOW} values increase smoothly as more channels are placed in O_2, and reach a broad maximum for $fO_2 = 0.8–0.9$. Thus, model 4 satisfies the adequacy test A, and predicts that both τ_{FAST} and A_{SLOW} will increase as more channels enter O_2.

Using rate constants determined at +60 mV and assuming all channels were in C_2 at rest, model 4 was run for various durations (Δt). The resulting distribution of channels among the five states was then recorded and used to define the initial conditions for running the model using −80 mV rate constants. The simulated tail currents thus obtained were then fit by double exponentials as before to obtain τ_{FAST} values. The predicted τ_{FAST} values from model 4 are shown together with those obtained at −80 mV from a GFL neuron for increasing duration depolarization to +60 mV (Fig. 7 *A*). This close agreement satisfies test B, as the appropriate channel distribution is established at positive voltages.

In addition, rate constants for model 4 at +40, +60, and +80 mV (Table 1) could account for the overall voltage-dependence of the gating transition at positive voltages. Values for the mean increase in τ_{FAST} are plotted in Fig. 7 *B* as a function of Δt for depolarization to +40 mV (*squares*), +60 mV (*circles*), and +80 mV (*diamonds*). Using model 4, τ_{FAST} values were determined for the appropriate voltage and are shown fitting the experimental data (*smooth curves*). The model also accounts for the relative absence of τ_{FAST} slowing for long pulses to 0 mV (*dashed line*).

Further indication of the adequacy of the voltage-dependence of rate constants (test C) was evaluated over a wide voltage range by the ability of the model to predict the kinetics of activation and deactivation. Ten-ms pulses to 0, +20, +40, and +60 mV were delivered in a GFL neuron, and are shown together with tail currents obtained after these pulses upon repolarization to −80 mV (Fig. 7 *C*, Data). Below, the simulations of model 4 are shown for the same voltages (Fig. 7 *C*, model 4). Recordings from most

neurons at positive voltages exhibited small outward "pedestal" currents from which inward current developed (see also currents in Fig. 1). It is unclear whether these currents arise from imperfect capacitance compensation, nonlinear ionic (leakage) currents, or from charge movement in ion channel proteins (gating currents). In any case, the model did not attempt to account for these early outward currents.

Following this initial period, however, $I_{Ca^{2+}}$ activation is well-described by the model, including the complex turn-on characteristics seen for pulses to 0, +20, and +40 mV (Fig. 7 *C*, model 4). The right side of this panel shows tail currents simulated at −80 mV using the final distribution of channels obtained at the end of the particular voltage pulse as the initial condition. The scaling factors for all modeled traces were obtained directly from the instantaneous $I_{Ca^{2+}}$-V relationship (see legend to Fig. 7).

Thus, model 4 satisfies the three tests of adequacy outlined earlier: 1) changing deactivation kinetics with one set of rate constants, 2) appropriate distribution of channels among these states to produce tail current slowing, and 3) voltage-dependent rate constants that accurately predict channel behavior.

Relief of ω-Aga IVA block

Ca^{2+} currents in GFL neurons are sensitive to block by the spider toxin ω-Aga IVA in the 10^{-7} M concentration range, and this block can be relieved by strong depolarization (Mintz et al., 1992; McFarlane and Gilly, 1996). Amplitudes and durations of these strongly depolarizing pulses are similar to those leading to the alterations in tail current kinetics described above. Moreover, the time course for development of these effects is similar, which raises the possibility that relief of ω-Aga IVA block is linked to the changing distribution of channels among the two presumptive open states.

Relief of ω-Aga IVA block is demonstrated in Fig. 8 *A*, which displays traces obtained with the voltage pulse protocol shown at the bottom. For both panels, currents were recorded in the presence (*black trace*) and absence (*gray trace*) of 500 nM ω-Aga IVA, which blocks 50–60% of $I_{Ca^{2+}}$ for these neurons. Current levels were recorded at the end of 10-ms pulses (*inset*) to 0 mV before (I_{pre}) and after (I_{post}) a variable duration (Δt) pulse to +60 mV, along with the tail currents recorded at −80 mV following I_{post}. The second pulse was delivered after a 10-ms step to −80 mV to allow channels to close after the strong pulse; this duration was insignificant compared with the time required to establish 500-nM ω-Aga IVA block (τ_{ON} = 64 ± 15 s, n = 7 neurons), and inclusion of this recovery period did not influence the results described below (comparison not shown).

The left panel demonstrates the blocking effect of 500-nM ω-Aga IVA, where currents during 10-ms pulses to 0 mV (I_{pre} and I_{post}) and total tail currents were diminished by the same factor. The fast component of the tail current appears to be blocked more effectively by ω-Aga IVA than the slow component (McFarlane and Gilly, 1996), but for these results only total tail current amplitudes are considered in regard to ω-Aga IVA block. A 10-ms pulse to +60 mV did not alter the level of block, as I_{pre} was equivalent to I_{post} in the presence of ω-Aga IVA. On the other hand, a 500-ms pulse to +60 mV (*right panel*) was able to completely relieve ω-Aga IVA block, as evidenced by the complete restoration of I_{post} in the presence of ω-Aga IVA to the control level. Relief is also visible in tail currents (slowed by the depolarizing prepulse) where $I_{Ca^{2+}}$ following the strong pulse is indistinguishable from its control counterpart.

For this neuron, the τ_{FAST} increase was determined for the same pulses in the absence of ω-Aga IVA, and is shown fitted with a single exponential (τ = 264 ms, Fig. 8 *B*). The time course of the relief of block was determined by computing the fractional increase in I_{post} (versus I_{pre}) for a pulse to +60 mV of Δt duration in the presence of 500 nM ω-Aga IVA. These values are shown in Fig. 8 *C*, along with a single exponential having a time constant of 257 ms, a value not significantly different from that describing the increase in τ_{FAST}.

This close temporal association of the relief of ω-Aga IVA block and the slowing of τ_{FAST} was consistently observed. The results inferred from the behavior of model 4 suggest that a slower τ_{FAST} seen after strong depolarization stems primarily from the increased occupancy of O_2. Inasmuch as depolarization causes both effects simultaneously, relief of ω-Aga IVA block may similarly depend on O_2 population. In other words, the blocking action of ω-Aga IVA on GFL $I_{Ca^{2+}}$ may be state-dependent.

To test this hypothesis, model 4 was modified to include ω-Aga IVA binding and unbinding transitions (model $4^{\dagger}$, Fig. 9 *A*), where ω-Aga IVA binding shifts channels into a "blocked" state. Because activation and deactivation kinetics of GFL $I_{Ca^{2+}}$ were not altered in the presence of ω-Aga IVA, model $4^{\dagger}$ assumes that gating transitions occur normally in blocked channels, but that blocked channels in either O_1 or O_2 do not pass current. The level of block is thus represented by the relative distribution of channels in "blocked" (*gray*) and "non-blocked" states (*black*). ω-Aga IVA associates reversibly with C_2, which is a reasonable assumption because the properties of block of GFL $I_{Ca^{2+}}$ are best explained by ω-Aga IVA binding to closed channels (see also Mintz et al., 1992). ON- (k_{ON}) and OFF-rates (k_{OFF}) were set to account for the slow onset of a half-blocking concentration of ω-Aga IVA observed in a single neuron (Fig. 9 *A*), and reproduced binding kinetics (τ_{ON} ~65 s) of 500-nM ω-Aga IVA. All states along the gating pathway possess an ω-Aga IVA binding step, but the bulk of the relief of ω-Aga IVA block at depolarizing potentials is presumed to occur via the step associated with blocked channels in O_2, and this OFF-rate (k_{OFF}, *thick arrow*) is presumed to be voltage-dependent and much faster than k_{ON} at positive potentials (*thin arrow*).

The voltage-dependence of relief of ω-Aga IVA block was determined by using the pulse protocol in Fig. 8 *A* for

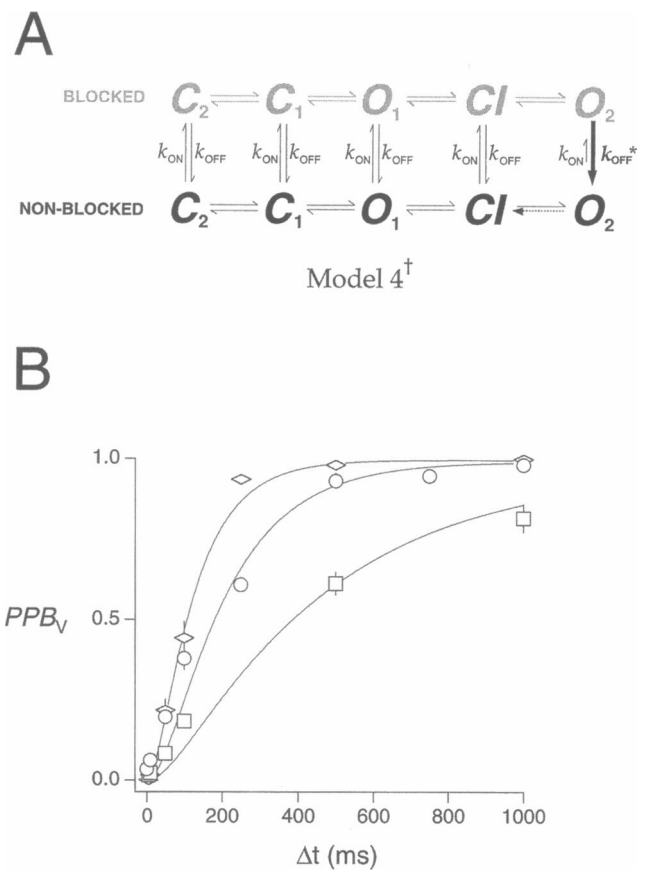

FIGURE 9 A modified version of model 4 (model 4†) can account for relief of ω-Aga IVA block. (*A*) Kinetic scheme of model 4†. The lower (black, "non-blocked") and upper (gray, "blocked") portions of model 4† are identical to model 4, and the same rate constants used for non-blocked channels were used for blocked channels (Table 1). Reversible ω-Aga IVA association steps are connected to all states along the gating pathway (ON-rate: k_{ON}; OFF-rate: k_{OFF}). k_{ON} and k_{OFF} were equal for all ω-Aga IVA binding reactions, and had values of 16.72 M^{-1} ms^{-1} and 7.02×10^{-6} ms^{-1}, respectively. The exception was the OFF-rate associated with O_2 (k_{OFF}*), which changed with voltage. The dashed arrow marking the $O_2 \rightarrow CI$ transition indicates that $k_{O_2\rightarrow CI}$ changes to obey microscopic reversibility. (*B*) Voltage-dependence of relief of ω-Aga IVA block. Relief of block was quantified as a voltage-dependent prepulse blocking index (PPB_V), using the equation, $PPB_V = (I_{post} - I_{Aga})/(I_{Ca^{2+}} - I_{Aga})$, where I_{Aga} and $I_{Ca^{2+}}$ represent Ca^{2+} current levels for a 10-ms pulse to 0 mV in the presence and absence of ω-Aga IVA, respectively. Mean (±SEM) PPB_V values measured from a number of GFL neurons (see text) are plotted as a function of prepulse duration (Δ*t*) to +40 mV (*squares*, $n = 4$), +60 mV (*circles*, $n = 7$), and +80 mV (*diamonds*, $n = 5$). k_{ON} and k_{OFF} were set to describe the time course of block of 500 nM ω-Aga IVA ($\tau_{ON} \sim 65$ s; $K_D \sim 420$ nM). Assuming all channels were in C_2 at rest, model 4† was run until equilibrium was reached. Calculations of model 4† for each voltage are shown fitting these data by substituting total tail current amplitude after the prepulse for I_{post} in the PPB_V relationship. Rate constants used for k_{OFF}* at −80, +40, +60, and +80 mV were 7.02×10^{-6}, 0.005, 0.014, and 0.03 ms^{-1}, respectively. The balancing rate constants for $k_{O_2\rightarrow CI}$ for these same voltages were 1.16, 1.30×10^{-4}, 3.01×10^{-5}, and 7.04×10^{-6} ms^{-1}, respectively.

interpulse voltages of +40, +60, and +80 mV. To evaluate both the time course and level of relief of block from a number of cells, a voltage-dependent prepulse blocking index (PPB_V) was established (see legend to Fig. 8). This index quantified the relief of block in the pulse (I_{post}) in comparison with the overall level of block produced by ω-Aga IVA in a single cell (10-ms pulse to 0 mV in the presence (I_{Aga}) and absence ($I_{Ca^{2+}}$) of ω-Aga IVA). A PPB_V value of 0.0 indicates that the prepulse had no effect, and a value of 1.0 represents complete restoration of the control $I_{Ca^{2+}}$ level. The time course of relief was observed to be largely independent of the level of ω-Aga IVA block, thus the PPB_V allows comparison of this time course among several GFL neurons.

Mean PPB_V values (±SEM) were calculated for prepulses to +40 mV (*squares*), +60 mV (*circles*), and +80 mV (*diamonds*) in the presence of 250 nM to 1 μM ω-Aga IVA (Fig. 9 *B*). For prepulses to +40 mV, full relief of block is not observed for $\Delta t = 1000$ ms, and in one case, extension of the prepulse to $\Delta t = 2000$ ms failed to produce full relief of block (not shown). For +60 and +80 mV, >95% relief of ω-Aga IVA block is reached within 1000 ms, with prepulses to +80 mV producing faster relief. These PPB_V values are shown together with the simulations of model 4†. The simulation calculated the increase in amplitude of tail currents (proportional to any change in I_{post}) after depolarization to +40, +60, or +80 mV, and modeled PPB_V was determined based on I_{post}. The overall voltage-dependence of k^*_{OFF} is similar to the voltage-dependent OFF-rate predicted from a pharmacokinetic analysis of rat neuronal $I_{Ca^{2+}}$ (*e*-fold in ~30 mV for GFL versus ~22 mV, Mintz et al., 1992). These rate constants for ω-Aga IVA block of GFL $I_{Ca^{2+}}$ predict a 4300-fold increase in estimated K_D over the −80 to +80 mV range (420 nM to 1.8 mM); this increase is quite similar to the 5000-fold increase predicted for rat (2 nM to 10 μM; Mintz et al., 1992).

To obey the principle of microscopic reversibility, $k_{O_2\rightarrow CI}$ (*dashed arrow*, Fig. 9 *A*) values were adjusted; these reductions had no observable effect on $I_{Ca^{2+}}$ kinetics for short pulses, presumably because the overall entry of channels into O_2 was limited by the very slow $O_1 \leftrightarrow CI$ reaction. The net effect of these reductions was an increase in the steepness of the voltage-dependence of $k_{O_2\rightarrow CI}$, increasing from *e*-fold in ~55 mV in the absence of ω-Aga IVA to *e*-fold in ~17 mV in the presence of toxin. Slower $k_{O_2\rightarrow CI}$ values in the presence of ω-Aga IVA lead to slower $I_{Ca^{2+}}$ resettling, especially at 0 mV, where $k_{O_2\rightarrow CI}$ values increase 150-fold. Such a mechanism might be responsible for the complex resettling of $I_{Ca^{2+}}$ at 0 mV following strongly depolarizing pulses of intermediate length in the presence of ω-Aga IVA (refer to Fig. 3 *C*, $\Delta t = 25$ and 100 ms; McFarlane and Gilly, 1996). A more realistic scheme, however, could be an allosteric model in which toxin affinity decreases in a graded fashion from left to right, as changes in rate constants would be more evenly distributed among several transitions.

DISCUSSION

This study provides a mechanistic explanation for biexponential tail currents recorded from squid GFL Ca^{2+} channels. The major conclusion drawn from the kinetic model proposed here is that the characteristics of deactivation are dependent on the proportion of channels closing from a second open state. Furthermore, the time-dependence of this effect is similar to the time course of relief of ω-Aga IVA block, suggesting a causal link between depolarization-induced slowing of tail currents and ω-Aga IVA unbinding from the channel. These observations seem to point to a novel form of voltage-dependent modification of neuronal Ca^{2+} channels, where prior depolarization leads to slower channel deactivation.

In a previous communication, it was assumed that fast and slow tail currents were generated by independent Ca^{2+} channel populations to investigate the localization of fast-deactivating ("FD") Ca^{2+} channels to extrasomatic domains of GFL neurons (McFarlane and Gilly, 1996). This convention was adopted because the fast component of deactivation exhibits similar kinetics to $I_{Ca^{2+}}$ expressed at the squid giant synapse (Llinás et al., 1981a). The experimental data presented here, however, more strongly suggest the presence of a single-channel species. Both fast and slow components of tail currents demonstrate sensitivity to external Ca^{2+}. In addition, both fast and slow tails possess closing rates that exhibit similar voltage dependence and contribute the same proportional fraction to tail currents at different voltages. More significantly, however, is that both fast and slow tail current components exhibit the same voltage-dependence of steady-state inactivation. This differs significantly for the case of fast and slow Ca^{2+} tail currents in mammalian systems (Cota, 1986; Matteson and Armstrong, 1986).

Effects of maintained depolarization, however, provide the strongest support for the existence of a single Ca^{2+} channel population. Full channel activation, which is reached when tail current amplitude no longer increases (Cota, 1986), can be achieved with relatively short duration strong pulses (+60 mV, 5–10 ms). For these short pulses, tail currents are primarily fast. For longer pulses, tail currents become slow, as the slow component grows in amplitude and the fast component decay rate decreases. A critical observation is that this changeover takes place without a change in total tail current amplitude. For two independently operating populations of Ca^{2+} channel to explain these data, increased activation of the more slowly deactivating channel would have to occur simultaneously with an inactivation of fast-deactivating channels. A similar mechanism has been used to account for the increase in sodium conductance in squid axon after a prepulse: the increased conductance was due to the late activation of "sleepy" sodium channels (Matteson and Armstrong, 1982). This precisely coordinated behavior is less likely to be present for GFL Ca^{2+} channels because of the preservation of tail current amplitude with increasing pulse length. Multi-open state gating (model 4) provides a more salient explanation for the fast-to-slow tail current shift.

Peculiar Ca^{2+} channel gating caused by strong depolarization has been observed in several different cell types. For 1,4-dihydropyridine (DHP)-sensitive Ca^{2+} channels of mammalian skeletal (Fleig and Penner, 1995), cardiac (Pietrobon and Hess, 1990) and smooth muscle (Nakayama and Brading, 1993), increasing pulse length causes the delayed activation of a Ca^{2+} conductance that contributes to tail currents. The data obtained from skeletal muscle Ca^{2+} channels were interpreted as arising from two separate populations of Ca^{2+} channel with different activation kinetics (Fleig and Penner, 1995). These data were explained by the presence of a "silent" Ca^{2+} conductance: channels are activated at positive voltages but do not pass current because membrane repolarization is required for current to flow (Fleig and Penner, 1995). On the other hand, Ca^{2+} channels from smooth muscle were postulated to behave as a single population, with strong depolarization causing channels to shift to a second open state (Nakayama and Brading, 1993). Channels closing from this second open state were presumed to be responsible for increased tail current amplitude and fivefold slower deactivation kinetics (Nakayama and Brading, 1993). In mammalian cerebellar (Slesinger and Lansman, 1991; Forti and Pietrobon, 1993) and hippocampal (Kavalali and Plummer, 1994) neurons, single DHP-sensitive Ca^{2+} channels display a different response to depolarization. After a strong prepulse, the open probability (P_o) of single Ca^{2+} channels increases substantially at test pulse voltages where P_o is normally small.

These voltage-dependent modifications all involve changes in gating of DHP-sensitive Ca^{2+} channels. Treatment with DHP agonists has been shown to increase "reopening" probability of single channels (Kavalali and Plummer, 1994) and exacerbate the depolarization-induced increase in whole-cell tail current amplitude (Nakayama and Brading, 1995). Similarly, DHP antagonists can block tail currents resulting from the slow voltage-dependent activation of a second Ca^{2+} conductance (Fleig and Penner, 1995).

The state transition described here diverges from this generalization, because GFL Ca^{2+} channels, like those at the presynaptic element of the squid giant synapse (Charlton and Augustine, 1990) are insensitive to block by dihydropyridine antagonists, including nifedipine (unpublished observations). Nevertheless, the basic observation that GFL $I_{Ca^{2+}}$ tends to deactivate more slowly after strong depolarization may be qualitatively similar to prepulse-induced increases in open probability on repolarization of DHP-sensitive Ca^{2+} channels observed on the microscopic level (Pietrobon and Hess, 1990; Slesinger and Lansman, 1991; Forti and Pietrobon, 1993; Kavalali and Plummer, 1994).

Properties of the Ca^{2+} channel response to strong depolarization in GFL neurons also differs from the cases of voltage-dependent gating modulation presented above, in that the GFL response is restricted exclusively to the deactivation process. $I_{Ca^{2+}}$ amplitude assessed with test pulses to

potentials where channel P_o is significant (e.g., 0 mV) appears unchanged by prior depolarization (see Fig. 5). Increases in $I_{Ca^{2+}}$ observed when performing standard prepulse protocols are transient, and represent the rapid deactivation of additional channels opened during the prepulse (McFarlane and Gilly, 1996). The control steady-state $I_{Ca^{2+}}$ is reached a few milliseconds after termination of the prepulse. In contrast, pulses delivered at voltages where P_o is low (≤ -20 mV) reveal significant delays in channel closing (see Fig. 5).

The essential features of the pulse length-dependent deactivation of GFL Ca^{2+} channels were adequately described by a two-open-state Markov-type kinetic model (model 4). Model 4 adequately described the main characteristics of this voltage-dependent gating transition by analyzing channel activation/deactivation at two potentials: -80 mV to measure tail currents and $+60$ mV to activate channels. The model was capable of predicting the fast activation of total $I_{Ca^{2+}}$, the presence of a slow tail current component for short duration pulses whose amplitude increased for long pulses, and the associated slowing of fast tail current decay. Given the constraints outlined in the kinetic modeling section, model 4 represents the minimal number of states necessary to explain the experimental data presented here.

The precise nature of the open states, O_1 and O_2, remains unclear in the absence of single-channel data. Model 4 assumed that O_1 and O_2 had the same unitary conductance because no evidence exists to suggest the presence of a subconductance state. However, this does not have to be the case. For model 4, if the conductance of O_2 were less than O_1, the macroscopic current appeared to inactivate as more channels entered O_2 with longer pulses. Indeed, subconductance states may provide the basis for fast inactivation of GFL neuron potassium channels (Mathes et al., 1996). Because GFL $I_{Ca^{2+}}$ inactivates very slowly, equal unitary conductances were used to determine rate constants, but single-channel recording may provide a definitive answer concerning this issue.

A conclusion drawn from the behavior of model 4 is that slow tails are a normal consequence of channel opening. Even for short pulses ($\sim$10 ms) to moderately depolarizing potentials (0 mV), the slow component represents a measurable fraction of the total tail current. Long pulses to 0 mV, however, produce neither a further increase in the amplitude of the slow component, nor a slowing of τ_{FAST}, nor a change in the efficacy of ω-Aga IVA block (not shown). This is a further indication that entry to O_2 increases with voltage, and that channels that close from O_2 are responsible for generating tail currents with increased A_{SLOW} components and slower τ_{FAST} values.

Relief of Ca^{2+} channel block with strong depolarization appears to be specific for ω-Aga IVA (Mintz et al., 1992), because similar relief cannot be produced for another peptide fraction of the same venom (ω-Aga IIIA; Mintz, 1994), or for an ω-conotoxin (Randall and Tsien, 1995). Like ω-Aga IVA block of cerebellar Purkinje neuron $I_{Ca^{2+}}$ (Mintz et al., 1992), relief of GFL $I_{Ca^{2+}}$ block appears to result from the physical displacement of toxin from its binding site because the reblocking kinetics exhibit a comparably slow time course to that seen for establishment of block for a given dose (unpublished observations). These results are qualitatively similar to the depolarization-induced relief of *Leiurus* α-toxin block of sodium channels (Strichartz and Wang, 1986). Like ω-Aga IVA for Ca^{2+} channels, relief of block by these scorpion toxins may be coupled to sodium channel gating (Strichartz and Wang, 1986).

Strong depolarization caused relief of ω-Aga IVA block with the same rate as the increase in τ_{FAST}. Results of simulation using model 4† suggest that toxin unbinding takes place as channels accumulate in state O_2 with increasing pulse length. In addition, the voltage-dependence of relief of ω-Aga IVA block is largely determined by the voltage-dependence of O_2 entry, with the amount of relief correlating with the degree of the τ_{FAST} increase. Taken together, these two results suggest the presence of "state-dependent" ω-Aga IVA block of GFL $I_{Ca^{2+}}$, in which ω-Aga IVA affinity is reduced for channels in state O_2 versus O_1. Depolarization-induced relief of ω-Aga IVA block may thus occur by a combination of state-dependent block and electrorepulsion of the positively charged toxin from its binding site on the extracellular surface of the Ca^{2+} channel protein (Mintz et al., 1992). That ω-Aga IVA block is so similar between GFL and P-type Ca^{2+} channels raises the intriguing possibility that other non-DHP-sensitive but ω-Aga IVA-sensitive neuronal Ca^{2+} channels exhibit anomalous gating similar to that described for GFL neurons.

Finally, the biphasic deactivation of GFL Ca^{2+} channels could be an important mechanism for evaluation of stimuli at the motor terminals of the giant axon, where channels of this type may be expressed in vivo (McFarlane and Gilly, 1996). GFL $I_{Ca^{2+}}$ shares many biophysical and pharmacological properties with $I_{Ca^{2+}}$ recorded at the presynaptic digits of the squid giant synapse. Tail currents recorded in this preparation have shown to be important for synchronization of the postsynaptic response as the driving force for Ca^{2+} entry increases after membrane repolarization (Llinás et al., 1981b). Tail currents with a slower rate of decay might cause a less temporally distinct rise in intracellular Ca^{2+} that could modulate the amount of residual presynaptic Ca^{2+} following strong or repetitive stimuli (Charlton et al., 1982; Swandulla et al., 1991). Slower channel deactivation may provide a basis for a presynaptic mechanism underlying the accumulation of Ca^{2+} ions necessary for short-term enhancement of synaptic efficacy (Delaney and Tank, 1994).

I am indebted to Dr. William F. Gilly for his support, advice, and encouragement throughout the course of this study. I also thank Drs. Richard Aldrich, Stephen Smith, and Richard Tsien for helpful discussions.

ω-Aga IVA was kindly provided by Pfizer, Inc.

This work was supported by National Institutes of Health Grant NS 17510 and a predoctoral fellowship from the Ford Foundation.

REFERENCES

Armstrong, C. M., and D. R. Matteson. 1984. Sequential models of sodium channel gating. *Curr. Top. Membr. Trans.* 22:331–352.

Artalejo, C. R., D. J. Mogul, R. L. Perlman, and A. P. Fox. 1991. Three types of bovine chromaffin cell Ca^{2+} channels: facilitation increases the opening probability of a 27 pS channel. *J. Physiol.* 444:213–240.

Augustine, G. J., M. P. Charlton, and S. J. Smith. 1987. Calcium action in synaptic transmitter release. *Annu. Rev. Neurosci.* 10:633–693.

Brown, A. M., Y. Tsuda, and D. L. Wilson. 1983. A description of activation and conduction in calcium channels based on tail and turn-on current measurements in the snail. *J. Physiol.* 344:549–583.

Byerly, L., and S. Hagiwara. 1982. Calcium currents in internally perfused nerve cell bodies of *Limnea stagnalis*. *J. Physiol.* 322:503–528.

Charlton, M. P., and G. J. Augustine. 1990. Classification of presynaptic calcium channels at the squid giant synapse: neither T-, L- nor N-type. *Brain Res.* 525:133–139.

Charlton, M. P., S. J. Smith, and R. S. Zucker. 1982. Role of presynaptic calcium ions and channels in synaptic facilitation and depression at the squid giant synapse. *J. Physiol.* 323:173–193.

Chow, RH. 1991. Cadmium block of squid calcium currents. Macroscopic data and a kinetic model. *J. Gen. Physiol.* 98:751–770.

Cota, G. 1986. Calcium channel currents in pars intermedia cells of the rat pituitary gland. Kinetic properties and washout during intracellular dialysis. *J. Gen. Physiol.* 88:83–105.

Delaney, K. R., and D. W. Tank. 1994. A quantitative measurement of the dependence of short-term synaptic enhancement on presynaptic residual calcium. *J. Neurosci.* 14:5885–5902.

Eckert, R., and D. Ewald. 1983. Calcium tail currents in voltage-clamped intact nerve cell bodies of *Aplysia californica*. *J. Physiol.* 345:533–548.

Fleig, A., and R. Penner. 1995. Excessive repolarization-dependent calcium currents induced by strong depolarizations in rat skeletal myoballs. *J. Physiol.* 489:41–53.

Forti, L., and D. Pietrobon. 1993. Functional diversity of L-type calcium channels in rat cerebellar neurons. *Neuron.* 10:437–450.

Hille, B. 1968. Charges and potentials at the nerve surface. Divalent ions and pH. *J. Gen. Physiol.* 51:221–236.

Hoshi, T., and S. J. Smith. 1987. Large depolarization induces long openings of voltage-dependent calcium channels in adrenal chromaffin cells. *J. Neurosci.* 7:571–580.

Hoshi, T., W. N. Zagotta, and R. W. Aldrich. 1994. Shaker potassium channel gating I. Transitions near the open state. *J. Gen. Physiol.* 103:249–278.

Kavalali, E. T., and M. R. Plummer. 1994. Selective potentiation of a novel calcium channel in rat hippocampal neurons. *J. Physiol.* 480:475–484.

Lláno, I., and R. J. Bookman. 1986. Ionic conductances of squid giant fiber lobe neurons. *J. Gen. Physiol.* 88:543–569.

Llinás, R., I. Z. Steinberg, and K. Walton. 1981a. Presynaptic calcium currents in squid giant synapse. *Biophys. J.* 33:289–322.

Llinás, R., I. Z. Steinberg, and K. Walton. 1981b. Relationship between presynaptic calcium current and postsynaptic potential in squid giant synapse. *Biophys. J.* 33:323–352.

Llinás, R., M. Sugimori, and R. B. Silver. 1992. Microdomains of high calcium concentration in a presynaptic terminal. *Science.* 256:677–679.

Mathes, C., J. J. Rosenthal, C. M. Armstrong, and W. F. Gilly. 1996. Similar potassium channel inactivation kinetics exist in squid giant axon and giant fiber lobe cell bodies. *Biophys. J.* 70:188*a*. (Abstr.)

Matteson, D. R., and C. M. Armstrong. 1982. Evidence for a population of sleepy sodium channels in squid axon at low temperature. *J. Gen. Physiol.* 79:739–758.

Matteson, D. R., and C. M. Armstrong. 1986. Properties of two types of calcium channels in clonal pituitary cells. *J. Gen. Physiol.* 87:161–182.

McFarlane, M. B., and W. F. Gilly. 1996. Spatial localization of calcium channels in giant fiber lobe neurons of the squid (*Loligo opalescens*). *Proc. Natl. Acad. Sci. USA* 93:5067–5071.

Mintz, I. M. 1994. Block of Ca channels in rat central neurons by the spider toxin w-Aga IIIA. *J. Neurosci.* 14:2844–2853.

Mintz, I. M., M. E. Adams, and B. P. Bean. 1992. P-type calcium channels in rat central and peripheral neurons. *Neuron.* 9:85–95.

Nakayama, S., and A. F. Brading. 1993. Evidence for multiple open states of the Ca^{2+} channels in smooth muscle cells isolated from the guinea-pig detrusor. *J. Physiol.* 471:87–105.

Nakayama, S., and A. F. Brading. 1995. Interaction of Ca^{2+} agonist and depolarization on Ca^{2+} channel current in guinea pig detrusor cells. *J. Gen. Physiol.* 106:1211–1224.

Pietrobon, D., and P. Hess. 1990. Novel mechanism of voltage-dependent gating in L-type calcium channels. *Nature.* 346:651–655.

Randall, A., and R. W. Tsien. 1995. Pharmacological dissection of multiple types of Ca^{2+} channel currents in rat cerebellar granule neurons. *J. Neurosci.* 15:2995–3012.

Slesinger, P. A., and J. B. Lansman. 1991. Reopening of Ca^{2+} channels in mouse cerebellar neurons at resting potentials during recovery from inactivation. *Neuron.* 7:755–762.

Smith, S. J., J. Buchanan, L. R. Osses, M. P. Charlton, and G. J. Augustine. 1993. The spatial distribution of calcium signals in squid presynaptic terminals. *J. Physiol.* 472:573–593.

Strichartz, G. R., and G. K. Wang. 1986. Rapid voltage-dependent dissociation of scorpion α-toxins coupled to Na channel inactivation in amphibian myelinated nerves. *J. Gen. Physiol.* 88:413–435.

Swandulla, D., and C. M. Armstrong. 1988. Fast-deactivating calcium channels in chick sensory neurons. *J. Gen. Physiol.* 92:197–218.

Swandulla, D., M. Hans, K. Zipser, and G. J. Augustine. 1991. Role of residual calcium in synaptic depression and posttetanic potentiation: fast and slow calcium signaling in nerve terminals. *Neuron.* 7:915–926.

Taylor, W. R. 1988. Two-suction-electrode voltage-clamp analysis of the sustained calcium current in cat sensory neurones. *J. Physiol.* 407: 405–432.

Zhou, W., and S. W. Jones. 1995. Surface charge and calcium channel saturation in bullfrog sympathetic neurons. *J. Gen. Physiol.* 105:441–462.